Mechanism of Regulation of *Acanthamoeba* Myosin-IC by Heavy-Chain Phosphorylation†

E. Michael Ostap,*,‡ Tianming Lin,‡ Steven S. Rosenfeld,§ and Nanyun Tang‡

Department of Physiology and The Pennsylvania Muscle Institute, University of Pennsylvania School of Medicine, 3700 Hamilton Walk, Philadelphia, Pennsylvania 19104-6085, and Department of Neurology, University of Alabama, Birmingham, Alabama 35294

Received May 30, 2002; Revised Manuscript Received August 21, 2002

ABSTRACT: The ATPase activity of myosin-Is from lower eukaryotes is activated by phosphorylation by the p21-activated kinase family at the TEDS site on an actin-binding surface-loop. This actin-binding loop is the site of a cardiac myosin-II mutation responsible for some forms of familial hypertrophic cardiomyopathy. To determine the mechanism of myosin-I regulation by heavy-chain phosphorylation (HCP) and to better understand the importance of this loop in the function of all myosin isoforms, we performed a kinetic investigation of the regulatory mechanism of the *Acanthamoeba* myosin-IC motor domain (MIC^{IQ}). Phosphorylated and dephosphorylated MIC^{IQ} show actin-activated ATPase activity; however, HCP increases the ATPase activity >20-fold. HCP does not greatly affect the rate of phosphate release from MIC in the absence of actin, as determined by single turnover experiments. Additionally, HCP does not significantly affect the affinity of myosin for actin in the absence or presence of ATP, the rate of ATP-induced dissociation of actoMIC^{IQ}, the affinity of ADP, or the rate of ADP release. Sequential-mix single-turnover experiments show that HCP regulates the rate of phosphate release from actin-bound MIC^{IQ}. We propose that the TEDS-containing actin-binding loop plays a direct role in regulating phosphate release and the force-generating (A-to-R) transition of myosin-IC.

Myosin-I is the single-headed low-molecular-weight member of the myosin superfamily (*1*). Members of the myosin-I family play roles in membrane dynamics, cell structure, and mechanical signal transduction (*2*−*7*). The kinetic mechanisms of all characterized myosin-Is follow the same pathway with the same biochemical intermediates (*8*−*10*). However, considerable kinetic variability exists within the myosin-I family (*11*, *12*).

ATPase activities of myosin-I isoforms from lower eukaryotes are activated by heavy-chain phosphorylation (HCP)[1] on a myosin surface-loop that interacts with actin (reviewed in *13*). A single serine or threonine (depending on the myosin isoform) on this loop is phosphorylated by members of the p21-activated kinase family (*14*−*16*). Myosins that are not regulated by HCP (including vertebrate myosin-Is) have a glutamate or aspartate at this site, suggesting that a negative charge at this position is important for activation (*17*). Because a threonine, aspartate, glutamate, or serine is almost always present at this position across the myosin superfamily, this amino acid position is called the TEDS site (*17*). Replacing serine residues with aspartate or glutamate residues at the TEDS sites of *Acanthamoeba* and *Aspergillus* myosin-Is activate ATPase activity (*18*, *19*). However, despite the conservation of charge at this position, a negative charge is not mandatory for the ATPase activity of all myosin isoforms (*10*, *20*).

The actin-binding loop containing the TEDS site is also of great interest because it is the location of a lethal mutation in the cardiac β-myosin heavy chain in patients with familial hypertrophic cardiomyopathy (*21*). Biochemical (*22*−*24*) and physiological (*25*) measurements of myosins with this mutation show significant alterations in mechanical and biochemical function. However, the biochemical steps altered by mutations at this loop are not known.

To determine the mechanism of regulation of myosin-I by HCP and to better understand the function of this loop in all myosin isoforms, we performed a kinetic characterization of phosphorylated and dephosphorylated myosin-IC. We found HCP affects directly the rate of phosphate release without greatly affecting the actin affinity, or the other key rate constants on the ATPase pathway (*8*).

EXPERIMENTAL PROCEDURES

Reagents, Proteins, and Buffers. *N*-Methyanthraniloyl (mant) ATP was synthesized as described (*26*). ATP and ADP concentrations were determined spectrophotometrically before each experiment by absorbance at 259 nm, $\epsilon_{259} = 15\,400\ M^{-1}\ cm^{-1}$. MantATP concentrations were determined by absorbance at 255 nm, $\epsilon_{255} = 23\,300\ M^{-1}\ cm^{-1}$ (*26*).

† This work was supported by National Institutes of Health Grant GM57247.

* Corresponding author. Address: Department of Physiology, B400 Richards, University of Pennsylvania School of Medicine, Philadelphia, PA 19104. Phone: 215-573-9758. Fax: 215-573-1171. E-mail: ostap@mail.med.upenn.edu. Web: http://www.med.upenn.edu/pmi.

‡ Department of Physiology and The Pennsylvania Muscle Institute.

§ University of Alabama.

[1] Abbreviations: P_iBP, fluorescently labeled phosphate binding protein; MIC^{IQ}, expressed myosin-IC protein construct containing a single IQ motif and bound light-chain; HCP, heavy-chain phosphorylation; mantATP, *N*-methyanthraniloyl-labeled ATP; K_{ATPase}, actin concentration at half-maximum of the steady-state ATPase rate; V_{max}, maximum actin-activated ATPase activity.

10.1021/bi0262193 CCC: $22.00
Published on Web 09/17/2002

Phosphate binding protein (P_iBP) was expressed, purified, and fluorescently labeled as described (*27*, *28*). Rabbit skeletal muscle actin was prepared and gel filtered (*29*). Actin concentrations were determined by absorbance at 290 nm, $\epsilon_{259} = 26\,600\ M^{-1}\ cm^{-1}$ (*30*). Actin was labeled with pyrenyl iodoacetamide (pyrene-actin) and gel filtered (*31*). All actin was stabilized with a molar equivalent of phalloidin (Sigma).

Steady-state and transient experiments were performed at 25 ± 0.2 °C in KMg10 buffer (10 mM imidazole, pH 7.0, 10 mM KCl, 1 mM $MgCl_2$, 1 mM EGTA, 1 mM DTT). We used KMg10, which is a low ionic strength buffer, to ensure interaction of the M·ADP·P_i state with actin at experimentally achievable protein concentrations.

Protein Expression and Purification. Recombinant baculovirus containing the cDNA for the myosin-IC motor domain and light chain were kindly provided by Dr. E. D. Korn (NIH, Bethesda, MD; identified as T2 in ref *32*). Myosin-IC was truncated at N720, generating a construct containing the motor domain and the only IQ motif (referred to as MIC^{IQ} throughout the text). The protein contains a FLAG epitope sequence at the N-terminus for purification (*32*).

MIC^{IQ} with bound light chain was purified from *Sf9* cells that were co-infected with virus containing recombinant MIC^{IQ} and light chain. Cells were suspended in lysis buffer (10 mM Tris, pH 7.0, 200 mM NaCl, 2 mM $MgCl_2$, 5 mM DTT, 1 mM PMSF, 0.01 mg/mL aprotinin, 0.01 mg/mL leupeptin), 2 mM ATP, and 0.05% Igepal at 4 °C and homogenized with 5 strokes in a Dounce homogenizer. Cell extract was centrifuged at 100 000*g* for 1 h. The supernatant was loaded onto anti-FLAG antibody columns (Sigma). Columns were washed with 5 column volumes of lysis buffer plus 2 mM ATP and 5 column volumes of lysis buffer. MIC^{IQ} was eluted with 10 mM Tris, pH 8.0, 100 mM NaCl, 1 mM DTT, 0.2 mg/mL FLAG peptide (Sigma), 0.01 mg/mL aprotinin, 0.01 mg/mL leupeptin. Eluted protein was phosphorylated with the catalytic fragment of myosin-I heavy-chain kinase as described (*33*) and loaded directly on to an 8 mL MonoQ column (Amersham Pharmacia) equilibrated in column buffer (10 mM Tris, pH 8.0, 25 mM KCl, 1 mM DTT) and eluted with a linear 25 mM−1 M KCl gradient. The Mono-Q column separated MIC^{IQ} from FLAG peptide and low concentrations of ADP and ATP. Fractions containing MIC^{IQ} were dialyzed versus 4 L (2 × 2 L) of 10 mM Tris, pH 7.5, 250 mM KCl, 1 mM EGTA, 1 mM DTT to remove contaminating nucleotide followed by dialysis versus storage buffer (10 mM Tris, pH 7.5, 100 mM KCl, 1 mM EGTA, 1 mM DTT, 50% glycerol), which concentrated the protein and allowed for storage at −20 °C.

The catalytic domain of myosin-I heavy-chain kinase (cDNA provided by H. Higgs and T. D. Pollard; Yale University) was expressed in bacteria (BL21(DE3) pLysS). Cells were grown to $OD_{600} = 0.5$ and induced with 1 mM IPTG for 2 h. Longer induction times resulted in lower kinase activity. Cells were suspended in kinase lysis buffer (20 mM Tris, pH 8.0, 20 mM KCl, 1 mM DTT, and protease inhibitors) and lysed by sonication. Cell extract was centrifuged for 30 min at 100 000g. The supernatant was loaded on to a DEAE column equilibrated in 20 mM Tris, pH 8.0, 20 mM KCl, 1 mM DTT, and eluted with a 20−500 mM gradient. Column fractions were assayed for kinase activity using peptide PC9 as described (*33*). Fractions containing kinase activity were dialyzed overnight versus 50 mM KCl, 1 mM EGTA, 1 mM DTT, 1 mM PMSF, 2 mM KPO_4, pH 7.0, and loaded on to an hydroxyl apatite column equilibrated in the same buffer. The column was eluted with a 20−300 mM KPO_4 gradient. Fractions containing kinase activity were dialyzed versus 20 mM KCl, 1 mM EGTA, 1 mM DTT, 10 mM Tris, pH 8.0, and then eluted from a mono-Q column with a 20 mM−1 M KCl gradient. 50 μL aliquots of purified kinase were frozen in liquid N_2 and stored at −80 °C.

Scheme 1

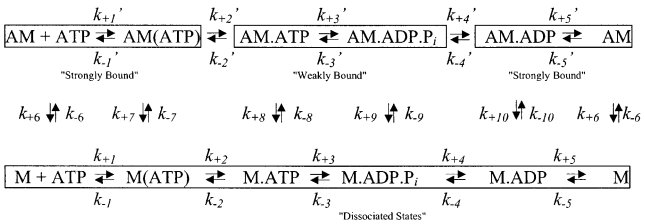

Before each experiment, concentrated phosphorylated MIC^{IQ} was incubated in dephosphorylation buffer (50 mM Tris, 1 mM $MnCl_2$, 5 mM DTT) in the absence or presence of ≤8000 units/mL λ protein phosphatase (New England Biolabs). Dephosphorylation of MIC^{IQ} was confirmed by steady-state ATPase activity.

Steady-State ATPase Activity and Sedimentation Assays. Steady-state ATPase activities were measured in KMg10 buffer at 25 °C using the NADH-coupled assay as described (*34*, *35*). Steady-state binding of 0.2 μM MIC^{IQ} to 0−70 μM actin was measured in KMg10 at 25 °C in the presence of 2 mM ATP by ultracentrifugation assays (350 000*g* for 20 min). The fraction of actin-bound myosin was determined by assaying the NH_4/EDTA ATPase activity of the supernatant (*36*).

Stopped Flow, Quenched-Flow, and Kinetic Modeling. Transient kinetic measurements were made at 25 ± 0.2 °C with an Applied Photophysics (Surrey, U.K.) SX.18MV stopped-flow fluorometer. A 400 nm filter was used to monitor pyrene and mantATP ($\lambda_{ex} = 365$ nm) fluorescence. Usually 2−8 transients were averaged before non-linear least-squares fitting. Experimental transients were fitted with software supplied with the instrument. Errors reported are standard errors in the fits.

Transient phosphate (P_i) release was measured using the coupled assay system containing the fluorescently labeled mutant of phosphate binding protein (*27*, *28*) with the stopped-flow in sequential mixing mode using a 440 nm long-pass filter ($\lambda_{ex} = 425$ nm). The dead time of the instrument in this configuration was ∼2 ms. Contaminating phosphate was removed from syringes, plastic ware, and the stopped-flow apparatus by incubating overnight with 0.5 mM 7-methylguanosine and 1 unit mL^{-1} nucleoside phosphorylase in KMg10. Background phosphate was removed from experimental solutions by incubating with 0.1 mM 7-methylguanosine and 0.02 unit mL^{-1} nucleoside phosphorylase.

Kinetic modeling and simulations were performed by modeling the reaction scheme of the actomyosin ATPase (Scheme 1) using Berkeley-Madonna (Robert I. Macey and George F. Oster; University of California, Berkeley).

RESULTS

Steady-State ATPase and Actin Binding Parameters. As shown for native and recombinant MIC (*32*), the steady-

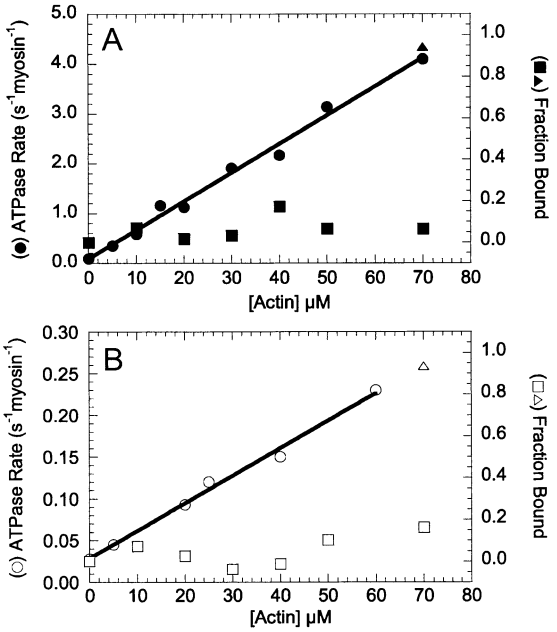

FIGURE 1: Steady-state ATPase and actin binding activity of (A) phosphorylated and (B) dephosphorylated MIC^{IQ}. (●, ○) Actin concentration dependence of the steady-state ATPase activity of 0.2 μM MIC^{IQ} in KMg10 measured using the NADH-coupled assay. The data points represent acquisitions from three different protein preparations, and the solid lines are linear fits of the data. The fraction of 0.1 μM MIC^{IQ} bound to actin in KMg10 in the (▲, △) absence and (■, □) presence of 2 mM ATP was measured by cosedimentation.

state ATPase activity of phosphorylated MIC^{IQ} is activated >50-fold by actin (Figure 1A, circles) while dephosphorylated MIC^{IQ} shows a much smaller actin activation (Figure 1B, circles). The ATPase rates of phosphorylated and dephosphorylated MIC^{IQ} are linearly related to the actin concentrations tested (Figure 1), indicating that the actin concentration at half-maximum of the steady-state ATPase rate (K_{ATPase}) is >70 μM. The slopes of the linear fits to the actin-activated ATPase rates are 0.06 μM^{-1} s^{-1} for phosphorylated MIC^{IQ} and 0.003 μM^{-1} s^{-1} for dephosphorylated MIC^{IQ}. We were not able to determine the maximum actin-activated ATPase activity (V_{max}) because of mixing problems due to high actin viscosity.

ATPase rates in the absence of actin were determined by single-turnover measurements using mant-ATP. The ATPase rate of phosphorylated MIC^{IQ} is 0.081 s^{-1} and 0.063 s^{-1} for dephosphorylated MIC^{IQ} (not shown; Table 1).

Steady-state actin-binding measurements show that phosphorylated (Figure 1A, squares) and dephosphorylated (Figure 1B, squares) MIC^{IQ} have very low actin affinities in the presence of ATP with <20% of phosphorylated or dephosphorylated MIC^{IQ} bound at 70 μM actin. Control reactions with rabbit skeletal myosin-II subfragment-1 (mixture of A1 and A2 isoforms) show ~50% binding at 70 μM actin under identical assay conditions (not shown).

MIC^{IQ} Binding to Actin Filaments. A ~60% fluorescence quenching upon strong binding of MIC^{IQ} to pyrene-actin allowed us to monitor the association of MIC^{IQ} with actin (*37*). Data were modeled as

$$AM \underset{k_{-6}}{\overset{k_{+6}}{\rightleftharpoons}} A^* + M \qquad (I)$$

Table 1: Rate and Equilibrium Constants for the MIC^{IQ} ATPase Cycle[a]

	phosphorylated MIC^{IQ}	dephosphorylated MIC^{IQ}
$K_1'k_{+2}'$ (μM^{-1} s^{-1})	3.3 (± 0.29)[b]	3.0 (± 0.20)[b]
$1/K_1'$ (μM)	260 (± 120)[b]	300 (± 85)[b]
k_{+2}' (s^{-1})	950 (± 190)[b]	870 (± 110)[b]
k_{+4}'/K_9' (μM^{-1} s^{-1})	0.08[c]	0.001[c]
K_9' (μM)	300[d]	300[d]
k_{+4}' (s^{-1})	24[e]	0.3[d]
k_{+4} (s^{-1})	0.081[f]	0.063[f]
K_6 (nM)	36 (± 7.0)[b]	47 (± 12)[b]
k_{-6} (μM^{-1} s^{-1})	6.9 (± 0.76)[b]	7.8 (± 0.57)[b]
K_5 (μM)	16 (± 0.3)[b]	12 (± 1.6)[b]
k_{+5} (s^{-1})	76 (± 3.0)[b]	73 (± 3.9)[b]

[a] KMg10 (10 mM KCl, 1 mM $MgCl_2$, 1 mM EGTA, 1 mM DTT, 10 mM Imidazole, pH 7.0, 25° C). [b] Pyrene-actin fluorescence. [c] Phosphate-binding protein. [d] Calculated (see text). [e] From ref *32* (see text). [f] Mant-ATP single turnover.

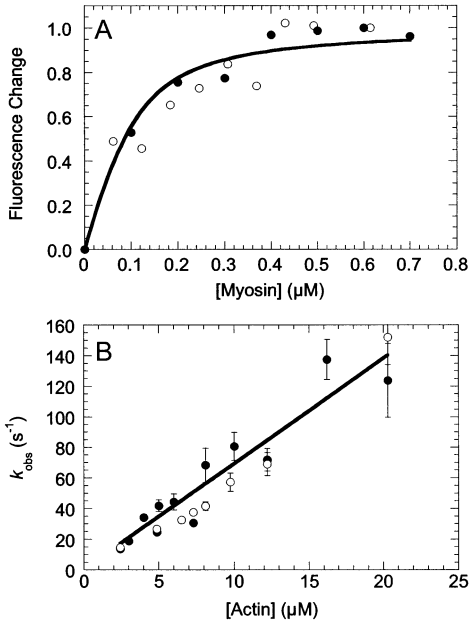

FIGURE 2: Kinetics of MIC^{IQ} association with actin filaments. (A) Steady-state titration of 0.1 μM pyrene-actin with (●) phosphorylated and (○) dephosphorylated MIC^{IQ}. The solid line is the best fit to the phosphorylated data using the binding equation defined in the Methods section. (B) Concentration dependence of the observed rate (k_{obs}) of pyrene-actin binding to 0.75 μM (●) phosphorylated and (○) dephosphorylated MIC^{IQ}. The data points represent acquisitions from two different protein preparations. The solid line is a linear fit to the phosphorylated data.

where A* represents the unquenched fluorescent state of pyrene-actin. The fluorescence signal from the equilibrium binding of MIC^{IQ} to pyrene-actin was normalized and fit (*8*, *37*), yielding dissociation constants of K_6 = 36 (± 7.0) nM for phosphorylated and K_6 = 47 (± 12) nM for dephosphorylated MIC^{IQ} (Figure 2A; Table 1).

Fluorescence time courses of MIC^{IQ} binding to pyrene-actin follow single exponential rates that depend linearly on the actin concentration (Figure 2B). Time courses of some protein preparations were best fit to two exponential rates. We report the fast rate in these cases (Figure 2B), and we attribute the slow rate to inactive protein because it was not present in all preparations. The apparent second-order rate constant for phosphorylated MIC^{IQ} binding to actin obtained from the slope is k_{-6} = 6.9 (± 0.76) μM^{-1} s^{-1}

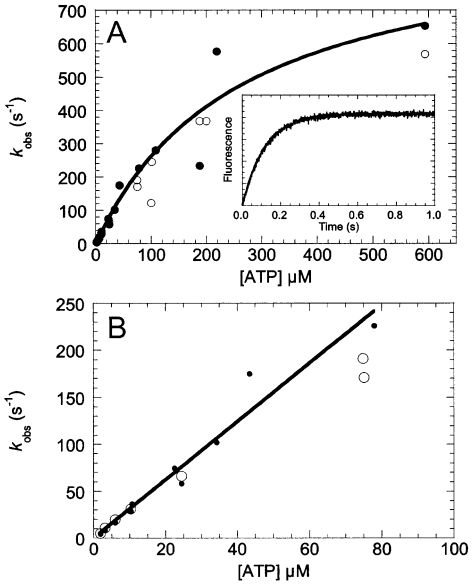

FIGURE 3: ATP-induced population of weakly bound actoMIC^{IQ} states. (A) ATP concentration dependence of the observed rate of dissociation (k_{obs}) of 0.5 μM actin from 0.5 μM (●) phosphorylated and (○) dephosphorylated MIC^{IQ} monitored by pyrene-actin fluorescence. All stopped-flow transients fit single exponentials. The solid line is a fit of the phosphorylated data to a rectangular hyperbola. The inset shows a pyrene-fluorescence transient obtained by mixing 0.5 μM actoMIC^{IQ} with 3 μM ATP. (B) Expanded graph shows k_{obs} is linearly related to the ATP concentration up to 50 μM ATP.

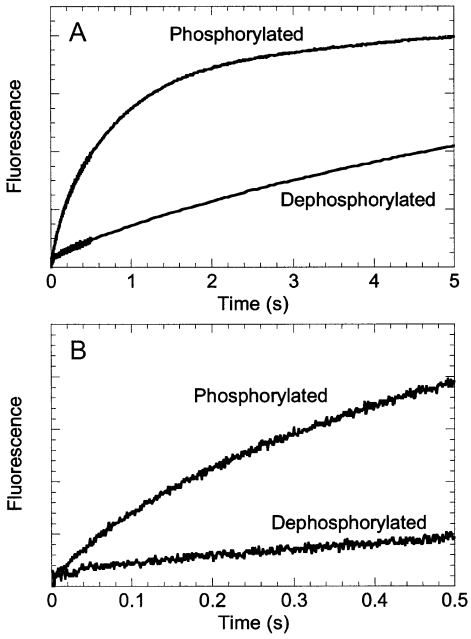

FIGURE 4: Phosphate release transients. (A) Time course of P_i release from phosphorylated and dephosphorylated MIC^{IQ} in the presence of actin after mixing with ATP in a sequential mix, single turnover experiment in KMg10. (B) Expanded region of transient showing the absence of burst or lag phases. Final concentrations at $t = 0$ were 5 μM P_iBP, 0.75 μM ATP, 1.5 μM MIC^{IQ}, 30 μM actin.

and 7.8 (± 0.57) μM^{-1} s^{-1} for dephosphorylated MIC^{IQ} (Table 1).

ATP-Induced Population of the Weakly-Bound States. Pyrene-actin fluorescence was used to monitor the ATP-induced population of the weakly bound states. Mixing ATP with pyrene-actoMIC^{IQ} results in an increase in fluorescence (Figure 3A, inset). Fluorescence transients were best fit to single exponentials at all ATP concentrations examined, and the rate of the fluorescence increase was hyperbolically related to the ATP concentration (Figure 3A). The mechanism of ATP-induced fluorescence enhancement was modeled as

$$AM + ATP \overset{K_1'}{\rightleftharpoons} AM(ATP) \xrightarrow{k_{+2}'} A^*M\cdot ATP \qquad (II)$$

where K_1' is a rapid equilibrium, k_{+2}' is a rate-limiting isomerization to the high fluorescence A*M·ATP state. When the ATP dependence on the observed rate is modeled as $k_{obs} = K_1'k_{+2}'[ATP]/([ATP]/K_1' + 1)$, $k_2' = 950$ (± 190) s^{-1}, and $1/K_1' = 260$ (± 120 uM) for phosphorylated MIC^{IQ} and $k_2' = 870$ (± 110) s^{-1} and $1/K_1' = 300$ (± 85 uM) for dephosphorylated MIC^{IQ} (Table 1). The association rate constant for ATP binding to phosphorylated actoMIC^{IQ} obtained from the initial slope ($K_1'k_2'$) is 3.3 (± 0.39) and 3.0 (± 0.20) μM^{-1} s^{-1} for dephosphorylated MIC^{IQ} (Figure 3B; Table 1).

Phosphate Release. Fluorescently labeled P_iBP was used to measure the rate of phosphate release (k_{+4} and k_{+4}') in sequential-mix, single-turnover, stopped flow experiments (Figure 4A; *10*, *12*, *27*). MIC^{IQ} (6 μM) was mixed with 3 μM ATP, aged for 1 s to allow for ATP binding and hydrolysis, and then mixed with 0−140 μM phalloidin-stabilized actin that was treated with apyrase to remove contaminating ADP and ATP. The final concentrations in the reaction cuvette were 1.5 μM MIC^{IQ}, 0.75 μM ATP, and 0−70 μM actin. P_iBP was included with the MIC^{IQ} and actin to prevent artifacts from phosphate released during the age time or phosphate contamination of the actin.

Time courses of phosphate release do not show lag or rapid burst phases (Figure 4B). The time courses of phosphate release from phosphorylated MIC^{IQ} in the presence of actin are best fit to the sum of two exponential rates (Figure 5A). The faster rate increased linearly with actin concentration (Figure 5A) and was >70% of the total fluorescent signal. The slower rate did not show a large actin-activation and likely reports phosphate release from inactive or dephosphorylated protein. The data were modeled using a two-step actin binding reaction (*10*):

$$\begin{array}{ccc} AM\cdot ADP\cdot P_i & \xrightarrow{k_4'} & AM\cdot ADP + P_i \\ K_9 \downarrow\uparrow & & \\ M\cdot ADP\cdot P_i + A & & \end{array} \qquad (III)$$

where K_9 is a rapid equilibrium actin-binding step and k_{+4}' is phosphate release. Phosphate release is irreversible in the presence of P_iBP, so k_{-4}' is not considered in the analysis (*10*). The rate of the fluorescence transient (k_{obs}) should depend hyperbolically on the actin concentration where $k_{obs} = k_{+4}'[A]/(K_9 + [A])$. The initial slope should yield an apparent second-order rate constant (k_{+4}'/K_9). We were not able to achieve high enough actin concentrations to observe the hyperbolic dependence due to difficulties of actin viscosity. We predict that actin concentrations >300 μM would be required obtain such a curve (see Discussion). A linear fit of the data yields the apparent second-order rate constant $k_{+4}'/K_9 = 0.08$ μM^{-1} s^{-1} (Table 1).

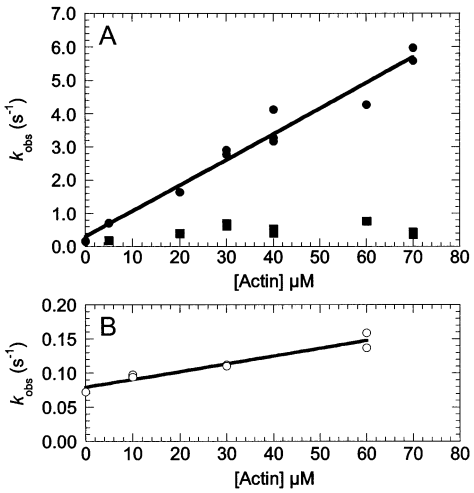

FIGURE 5: Phosphorylation and actin dependence of phosphate release. (A) Actin concentration dependence on the rate of phosphate release from phosphorylated MIC^{IQ}. The observed rates (k_{obs}) were determined by fitting the stopped-flow fluorescence transients at each actin concentration to the sum of two exponential rates. The solid line is the best linear fit of the fast rate. (B) Actin concentration dependence on the rate of phosphate release (k_{obs}) from dephosphorylated MIC^{IQ}. Transients were best fit to a single-exponential rate. For all experiments the delay time after first mix = 1 s. Final concentrations at $t = 0$ were 5 μM P_iBP, 0.75 μM ATP, 1.5 μM MIC^{IQ}, 0−70 μM actin.

The rates of phosphate release from dephosphorylated MIC^{IQ} are best fit to a single exponentials, and also show an actin-dependent increase (Figure 5B). A linear fit to the data yields a rate constant of $k_{+4}'/K_9 = 0.001\ \mu M^{-1}\ s^{-1}$ (Table 1).

ADP Binding and Release. The affinity of ADP for pyrene-actoMIC^{IQ} was determined by competitive binding with ATP as described by (*38*):

$$AM{\cdot}ADP \overset{K_5'}{\rightleftharpoons} AM + ATP \overset{K_1'}{\rightleftharpoons} AM(ATP) \xrightarrow{k_{+2}'} A^*M{\cdot}ATP \qquad \text{(IV)}$$

0.5 μM MIC^{IQ} bound to 5 μM pyrene-actin was incubated with varying concentrations of ADP and mixed with 47 μM ATP. Dephosphorylated and phosphorylated MIC^{IQ}·ADP were strongly bound to pyrene-actin, as determined by pyrene fluorescence. Fluorescence transients fit single-exponential rates that have a hyperbolic dependence on the ADP concentration (Figure 6A), indicating that the AM and AM·D states are in rapid equilibrium. Therefore, the dependence of k_{obs} on the ADP concentration is given by

$$k_{obs} = \frac{k_o}{1 + \left(\frac{[ADP]}{K_5'}\right)} \qquad (1)$$

where k_o is the rate of pyrene-actoMIC^{IQ} dissociation in the absence of ADP ($k_o = K_1'k_2'$[ATP]; reaction IV) and K_5' is the equilibrium dissociation constant for ADP (reaction IV). Fits to the data yield $K_5' = 16\ (\pm 0.3)\ \mu$M for phosphorylated MIC^{IQ} and $K_5' = 12\ (\pm 1.6)\ \mu$M for dephosphorylated MIC^{IQ} (Figure 6A).

The rate of ADP release (k_{+5}') was measured by incubating pyrene-actoMIC^{IQ} with 0.6 mM ADP and rapidly mixing with a large excess of ATP (Figure 6B). This concentration

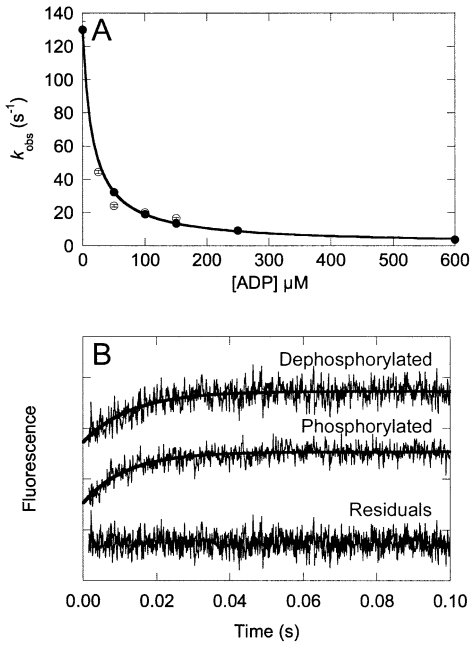

FIGURE 6: Kinetics of ADP binding and dissociation. (A) ADP concentration dependence on ATP-induced dissociation of pyrene-actoMIC^{IQ}. The observed rates (k_{obs}) were determined by fitting the stopped-flow transients to single-exponential rates. The solid line is the best fit of the data to eq 1. Final concentrations at $t = 0$ were 0.5 μM (●) phosphorylated or (○) dephosphorylated MIC^{IQ}, 5 μM pyrene-actin, 47 μM ATP, 0−600 μM ADP. (B) The rate of ADP release from (upper trace) dephosphorylated and (low trace) phosphorylated MIC^{IQ} measured by ATP-induced dissociation from pyrene-actin. The solid lines are the fits of the data to single-exponential functions with rates of 77 s^{-1} for dephosphorylated MIC^{IQ} and 85 s^{-1} for phosphorylated MIC^{IQ}. The residuals obtained by subtracting the best-fit exponential function from the dephosphorylated and phosphorylated data are shown overlaid. Final concentrations at $t = 0$ were 0.5 μM MIC^{IQ}, 5 μM pyrene-actin, 5 mM ATP, and 0.6 mM ADP.

of ADP should saturate the actoMIC^{IQ} active sites (Figure 6A; Table 1), and thus the rate of ADP release should limit the rate ATP binding and subsequent increase in pyrene-actin fluorescence (reaction IV). The fluorescence increase fit a single-exponential function with a rate of 76 (± 3.0) s^{-1} for phosphorylated and 73 (± 3.9) s^{-1} for dephosphorylated MIC^{IQ} (Figure 6B).

DISCUSSION

Overview of Myosin-IC ATPase and Regulation. The MIC^{IQ} rate constants (Table 1) are similar to other characterized subclass-1 myosin-I isoforms (*8*, *12*), and most of the rate constant are not affected by HCP. The actin dependence on the steady-state ATPase rate (Figure 1) is nearly identical to the actin dependence on the rate of phosphate release (Figure 5) for phosphorylated and dephosphorylated MIC^{IQ}. Actin activation of phosphate release (k_{+4}'/K_9) is the rate-limiting step at actin concentrations ≤70 μM, and phosphate release (k_{+4}') is likely rate limiting at very high actin concentrations. Therefore, HCP regulates the steady-state ATPase rate by regulating phosphate release.

Steady-state binding measurements show that less than 20% of MIC^{IQ} is bound to 70 μM actin in the presence of ATP (Figure 1), indicating a very weak actin affinity. If M·ADP·P_i is the predominant steady-state intermediate and if we assume that the maximum rate of phosphate release

(k_{+4}') is the same as the V_{max} of full-length myosin-IC (24 s^{-1}; *32*), then using data from Figure 5A ($k_{+4}'/K_9 = 0.08$ μM^{-1} s^{-1}), we calculate K_9 to be ~300 μM (Table 1). Under similar conditions, the actin affinity of the M·ADP·P_i is >100 μM for myo1e (*12*), ~20 μM for skeletal muscle myosin-II (*27*), and ~35 μM for myosin-VI (*10*). It was proposed that the weak actin affinity of the motor domain of myosin-I in the presence of ATP is the result of the low density of positive charge in loop-2 and is an adaptation to the high actin concentration environment in which myosin-I isoforms function (*12*).

The ATPase activity of dephosphorylated MIC^{IQ} is actin-activated (Figure 1B), i.e., it is not completely switched "off" by dephosphorylation (*18*, *19*, *32*). We are confident that this activation is not due to incomplete dephosphorylation of MIC^{IQ}, since a fast exponential phase due to phosphorylated protein is not observed in the phosphate release experiments (Figure 4B). We were not able to determine directly V_{max} for dephosphorylated MIC^{IQ}. However, if we assume that K_9 is not changed by heavy-chain phosphorylation (see below), then using the data from Figure 5B ($k_{+4}'/K_9 = 0.001$ μM^{-1} s^{-1}), we calculate k_{+4}' (and V_{max}) to be ~0.3 s^{-1}.

Regulation of the Weak-to-Strong Transition and Force Generation. Myosin binding to actin has been modeled to occur in three steps as described by Geeves, Goody, and Gutfreund (Scheme 2; *39*, *40*):

Scheme 2

$$\text{A + M.N} \;\overset{K_0^{3G}}{\leftrightarrow}\; \text{A~M.N} \;\overset{K_1^{3G}}{\leftrightarrow}\; \text{A-M.N} \;\overset{K_2^{3G}}{\leftrightarrow}\; \text{A.M.N}$$

Collision Complex — Attached (A) State — Rigor-like (R) State

(the 3G superscript is added to avoid confusion with Scheme 1). The formation of the collision complex (K_0^{3G}) is ionic-strength-dependent and nucleotide-independent (*34*, *39*). The isomerization to the A-state (K_1^{3G}) leads to the formation of stereospecific hydrophobic interactions and is also likely to be nucleotide independent (*39*). The A-to-R transition (K_2^{3G}) is thought to be coupled to the myosin power-stroke and is detected in solution biochemistry by the quenching of pyrene-actin fluorescence (*39*, *41*). K_2^{3G} is very sensitive to the bound nucleotide and is significantly decreased by the presence of the γ-phosphate of ATP (*40*).

The rate of association of nucleotide-free myosin (Figure 2B) is modeled as $k_{-6} = K_0^{3G}k_{+1}^{3G}$ (Scheme 2; *34*), where k_{-6} is defined in Scheme 1. Because HCP does not affect the rate of nucleotide free MIC^{IQ} binding, actin binding (K_0^{3G}) and the rate of population of the A-state (k_{+1}^{3G}) are probably not regulated for other MIC^{IQ} nucleotide states (*34*, *39*). Therefore, HCP regulation of phosphate release (k_4', Figure 5) is most likely a direct effect on the A-to-R transition (K_2^{3G}; Scheme 2). This proposal is supported by recent investigations of myosin-VI mutants that mimic phosphorylation at the TEDS site (see below), which show that the actin affinity of the M·ADP·P_i state (K_9, Scheme 1) is not dependent on the "phosphorylation state" of this site and that rate of M and M·ADP binding to actin are not affected by HCP (*10*).

Although the rate of phosphate release is significantly decreased by dephosphorylation (Table 1), the presence of actin-activated ATPase activity of dephosphorylated MIC^{IQ} suggests that the actin-bound motor produces a force-generating powerstroke (*42*). Because ADP release is not affected by HCP (Table 1) and the rate of ADP release limits actin sliding velocity (*43*), we predict that dephosphorylated myosin-IC will move actin filaments at the same rate as fully activated myosin-IC at high effective actin or myosin concentrations (assuming the nonforce generating myosins do not put a resisting force on the system). However, the very slow rate of phosphate release will decrease the frequency of force-generating powerstrokes from a single motor and thus will greatly decrease the total force from a group of motors.

Relationship to Other Myosins. Other than myosin-I isoforms from lower eukaryotes, the only other myosin predicted to be regulated at the TEDS site by the p21-activated kinase family is myosin-VI (*17*). A myosin-VI mutant that mimics TEDS phosphorylation has an increased rate of actin-activated phosphate release (*10*). However, the rate-limiting step of the myosin-VI ATPase is ADP release (k_5'; Scheme 1) for the phosphorylated and dephosphorylated mutants, so HCP does not affect the V_{max}. Additionally, HCP appears to regulate the rate of actin-activated phosphate release <3-fold (*10*), not the 80-fold regulation seen for myosin-IC (Table 1). Therefore, HCP phosphorylation of myosin-VI likely plays a modulatory role, possible affecting the duty ratio of myosin-VI and magnitude of processivity (*10*).

Vertebrate myosin-I isoforms are not predicted to be regulated by phosphorylation at the TEDS site (*17*), and direct measurements of the reactivity of myo1e with myosin-I heavy-chain kinase support this prediction (*12*). It has been demonstrated that tropomyosin regulates the motor activity (*44*, *45*) and the cellular localization of vertebrate myosin-I isoforms (*45*). Tropomyosin is thought to regulate the A-to-R transition of all myosins (*39*). Therefore, although the mechanism of myosin-I regulation differs between higher and lower eukaryotes, the same kinetic transition is regulated in both cases. Given our results (Table 1), it is interesting to note that the TEDS rule loop might be sterically regulated by tropomyosin in higher eukaryotes (*8*, *46*). Therefore, we propose that isoform differences in the sequence and structure of this loop affect the ability of myosin isoforms to be differentially regulated by tropomyosin.

Familial Hypertrophic Cardiomyopathy. The actin-binding loop containing the TEDS site is referred to as the "403" or "myopathy" loop. This is because a lethal R403Q missense mutation in cardiac muscle β-myosin-II occurs in this loop in some forms of familial hypertrophic cardiomyopathy (*21*). Measurements of myosins with this mutation show significant alterations in mechanical and biochemical function (*22*−*25*). Although the effect of this point mutation on myosin kinetics is likely dependent on the myosin isoform (*22*, *24*), our investigation indicates that alterations to this loop likely affect the rate of phosphate release and the force-generating (A-to-R; Scheme 2) transition. Alteration of the rate of phosphate release does not necessarily change the unitary force or step-size of a single myosin (*42*), but it does change the total force generated by a group of myosins, e.g., in a muscle fiber. Additionally, altering the rate of force generation (and the lifetime of force-producing states) affects the activation of tropomyosin-troponin regulated actin filaments. Therefore, we predict that the physiological effects of R403Q mutation

are the direct result of an alteration of the rate of the A-to-R transition. However, further biochemical experiments are required to better understand the biochemical consequence of the R403Q in cardiac myosin-II.

Conclusion. HCP activates phosphate release from actin-bound myosin-IC without significantly affecting the other key rate constants on the actomyosin-IC ATPase pathway. We propose that the TEDS-containing actin-binding loop plays a direct role in regulating phosphate release and the A-to-R (force-generating) transition in the presence of ATP for myosin-IC and all myosin isoforms.

ACKNOWLEDGMENT

We thank Dr. E. D. Korn and his laboratory for providing the MIC^{IQ} and light-chain virus and for helpful discussions, H. Higgs and T. D. Pollard for the cDNA for myosin-I light-chain kinase, M. A. Shaw and Y. E. Goldman for skeletal muscle S1, J. Poole and M. El Mezgueldi for assistance in the early phases of this project, and E. M. De La Cruz and C. Yengo for helpful discussions.

REFERENCES

1. Berg, J. S., Powell, B. C., and Cheney, R. E. (2001) *Mol. Biol. Cell 12*, 780−794.
2. Geli, M. I., and Riezman, H. (1996) *Science 272*, 533−535.
3. Jung, G., Wu, X., and Hammer, J. A., III (1996) *J. Cell Biol. 133*, 305−323.
4. Raposo, G., Cordonnier, M. N., Tenza, D., Menichi, B., Durrbach, A., Louvard, D., and Coudrier, E. (1999) *Mol. Biol. Cell. 10*, 1477−1494.
5. Dai, J., Ting-Beall, H. P., Hochmuth, R. M., Sheetz, M. P., and Titus, M. A. (1999) *Biophys. J. 77*, 1168−1176.
6. Novak, K. D., Peterson, M. D., Reedy, M. C., and Titus, M. A. (1995) *J. Cell Biol. 131*, 1205−1221.
7. Holt, J. R., Gillespie, S. K. H., Provance, D. W., Jr., Shah, K., Shokat, K. M., Corey, D. P., Mercer, J. A., and Gillespie, P. G. (2002) *Cell 108*, 371−381.
8. Ostap, E. M., and Pollard, T. D. (1996) *J. Cell Biol. 32*, 1053−1060.
9. De La Cruz, E. M., Wells A. L., Rosenfeld, S. S., Ostap, E. M., and Sweeney, H. L. (1999) *Proc. Natl. Acad. Sci. U.S.A. 96*, 13726−13731.
10. De La Cruz, E. M, Ostap, E. M., and Sweeney, H. L. (2001) *J. Biol. Chem. 276*, 32373−32381.
11. Jontes, J. D., Milligan, R. A., Pollard, T. D., and Ostap, E. M. (1997) *Proc. Natl. Acad. Sci. U.S.A. 94*, 14332−14337.
12. El Mezgueldi, M., Tang, N., Rosenfeld, S., and Ostap, E. M. (2002) *J. Biol. Chem. 277*, 21514−21521.
13. Barylko, B., Bins, D. D., and Albanesi, J. P. (2000) *Biochim. Biophys. Acta 1496*, 23−35.
14. Brzeska, H., Lynch, T. J., Martin, B., and Korn, E. D. (1989) *J. Biol. Chem. 264*, 19340−19348.
15. Lee, S.-F., Egelhoff, T. T., Mahasneh, A., and Côté, G. P. (1996) *J. Biol. Chem. 271*, 27044−27048.
16. Brzeska, H., Szczepanowska, J., Hoey, J., and Korn, E. D. (1996) *J. Biol. Chem. 271*, 27056−27062.
17. Bement, W. M., and Mooseker, M. S. (1995) *Cell Motil. Cytoskeleton 31*, 87−92.
18. Wang, Z,-Y., Wang, F., Sellers, J. R., Korn, E. D., and Hammer, J. A., III (1998) *Proc. Natl. Acad. Sci. U.S.A. 95*, 15200−15205.
19. Liu, X., Osherov, N., Yamashita, R., Brzeska, H., Korn, E. D., and May, G. S. (2001) *Proc. Natl. Acad. Sci. U.S.A. 98*, 9122−9127.
20. Wang, F., Harvey, E. V., Conti, M. A., Wei, D., and Sellers, J. R. (2000) *Biochemistry 39*, 5555−5560.
21. Rayment, I., Holden, H. M., Sellers, J. R., Fananapazir, L., and Epstein, N. D. (1995) *Proc. Natl. Acad. Sci. U.S.A. 92*, 3864−3868.
22. Cuda, G., Fananapazir, L., Epstein, N. D., and Sellers, J. R. (1997) *J. Muscle Res. Cell Motil. 18*, 275−283.
23. Roopnarine, O., and Leinwand, L. A. (1998) *Biophys. J. 75*, 3023−3030.
24. Tyska, M. J., Hayes, E., Giewat, M., Seidman, C. E., Seidman, J. G., and Warshaw, D. M. (2000) *Circ. Res. 86*, 737−744.
25. Lankford, E. B., Epstein, N. D., Fananapazir, L., and Sweeney, H. L. (1995) *J. Clin. Invest. 95*, 1409−1414.
26. Hiratsuka, T. (1983) *Biochim. Biophys. Acta 742*, 496−508.
27. White, H. D., Belknap, B., and Webb, M. R. (1997) *Biochemistry 36*, 11828−11836.
28. Brune, M., Hunter, J. L., Corrie, J. E., and Webb, M. R. (1994) *Biochemistry 30*, 8262−8271.
29. Spudich, J. A., and Watt, S. (1971) *J. Biol. Chem. 246*, 4866−4871.
30. Houk, T. W., and Ue, K. (1974) *Anal. Biochem. 62*, 66−74.
31. Pollard, T. D. (1984) *J. Cell Biol. 99*, 769−777.
32. Liu, X., Brzeska, H., and Korn, E. D. (2000) *J. Biol. Chem. 275*, 24886−24892.
33. Lynch, T. J., Brzeska, H., Baines, I. C., and Korn, E. D. (1991) *Methods Enzymol. 196*, 12−23.
34. Furch, M., Geeves, M. A., and Manstein, D. J. (1998) *Biochemistry 37*, 6317−6326.
35. De La Cruz, E. M., Sweeney H. L., and Ostap, E. M. (2000) *Biophys. J. 79*, 1524−1529.
36. Chalovich, J. M., and Eisenberg, E. (1982) *J. Biol. Chem. 257*, 2432−2437.
37. Geeves, M. A., and Jeffries, T. E. (1988) *Biochem. J. 256*, 41−46.
38. Geeves, M. A. (1989) *Biochemistry 28*, 5864−5871.
39. Geeves, M. A., and Connibear, P. B. (1995) *Biophys. J. 68*, 194s−201s.
40. Geeves, M. A.; K. C. Holmes (1999) *Annu. Rev. Biochem. 68*, 687−728.
41. Taylor, E. W. (1991) *J. Biol. Chem. 266*, 294−302.
42. Baker, J. E., Brosseau, C., Joel, P. B., and Warshaw, D. M. (2002) *Biophys. J. 82*, 2134−2147.
43. Siemankowski, R. F., Wiseman, M. O., and White, H. D. (1985) *Proc. Natl. Acad. Sci. U.S.A. 82*, 658−662.
44. Fanning, A. S., Wolenski, J. S., Mooseker, M. S., and Izant, J. G. (1994) *Cell Motil. Cytoskeleton 29*, 29−45.
45. Tang, N., and Ostap, E. M. (2001) *Curr. Biol. 11*, 1131−1135.
46. Holmes, K. C. (1995) *Biophys. J. 68*, 2s−7s.

BI0262193